Electrochemistry Communications 119 (2020) 106824

Contents lists available at ScienceDirect

Electrochemistry Communications

journal homepage: www.elsevier.com/locate/elecom

The role of Ru clusters in Fe carbide suppression for the reverse water gas shift reaction over electropromoted Ru/FeO_x catalysts

Christopher Panaritis[a], Johnny Zgheib[a], Martin Couillard[b], Elena A. Baranova[a,*]

[a] Department of Chemical and Biological Engineering, Centre for Catalysis Research and Innovation (CCRI), University of Ottawa, 161 Louis-Pasteur, Ottawa, ON K1N 6N5, Canada

[b] National Research Council of Canada, 1200 Montreal Road, Ottawa, ON K1A 0R6, Canada

ARTICLE INFO

Keywords:
Electrochemical promotion of catalysis
NEMCA
Reverse water–gas shift
Iron-oxide
Ruthenium
Iron-carbide

ABSTRACT

The formation of an iron carbide phase has been shown to inhibit the efficiency of Fe-based catalysts in the initial step of adsorbing carbon dioxide (CO_2). In this study, we evaluate the effect of adding Ru clusters (20% at.) to FeO_x nanowires deposited on yttria-stabilized zirconia (YSZ) for the reverse water gas shift (RWGS) reaction carried out at 300–400 °C under atmospheric conditions. STEM shows that Ru-FeO_x formed a bi-phase structure with Ru clusters (1.5–2 nm) supported on FeO_x nanowires (5 nm) that remain as mixed oxides after the reaction. Open-circuit catalytic measurements demonstrated that addition of Ru increased the catalytic activity and stabilized high selectivity (> 99%) towards CO. The synergetic effect of Ru and FeO_x was further emphasized through electrochemical polarization, which led to a reversible catalytic activity increase of up to 2.4 times. The addition of Ru inhibits the formation of inactive Fe carbide by acting as the reducing component and stabilizing the FeO_x active state. This results in an improved and lasting catalytic performance and makes Ru/FeO_x catalysts attractive for industrial applications.

1. Introduction

Given the importance of reducing the amount of carbon dioxide in the atmosphere and minimizing its effect on the environment, advances in current technology are required to convert CO_2 into useful chemicals [1]. The reverse water gas shift (RWGS) (R1) is a promising approach in the manufacture of carbon monoxide (CO) to be used in the Fischer–-Tropsch synthesis to produce carbon–neutral products [2,3]. Generating carbon–neutral products is a crucial transition from fossil fuels to a renewable economy [4].

$$CO_2 + H_2 \leftrightarrow CO + H_2O \quad \text{(R1)}$$

$$CO_2 + 4H_2 \rightarrow CH_4 + 2H_2O \quad \text{(R2)}$$

The difficulty of activating CO_2 can be overcome using heterogenous catalytic reactions. Ruthenium is widely used in the CO_2 hydrogenation reaction due to its ability to dissociate H_2 and CO_2, producing CO and methane (CH_4) (R2) [5–7]. The selectivity of the response of Ru can be tailored by its size, surface composition, doping and the catalyst support via the metal–support interaction (MSI) [8,9]. An electronic type of MSI has been reported for a number of active catalyst supports consisting of mixed ionic electronic or ionically conductive ceramics. The charge transfer between the catalyst and the support is often accompanied by the spontaneous migration of ionic species in the form of oxygen (O^{2-}), sodium ($Na^{\pm}$), potassium ($K^{\pm}$) or hydrogen ($H^{\pm}$), which is responsible for the observed high catalytic activity and selectivity [10,11]. Among these, oxygen conducting supports, such as doped ceria (Gd-CeO_2, Sm-CeO_2) and yttrium stabilized zirconia, (YSZ) have been shown to be viable and popular candidates for the RWGS reaction, due to their ability to cycle oxygen [12]. Pairing Ru nanoparticles with active supports provides a dual mechanism in which Ru dissociates H_2 into atomic H, where it is able to spill over on the support to reduce it and generate oxygen vacancies [13]. Iron (Fe), or more specifically Fe oxides (FeO_x) (Fe_3O_4 and FeO) have the ability to cycle oxygen through redox reactions [14] and are active towards the RWGS reaction as the first step in reducing CO_2 to CO, which has been determined to be the intermediate species in most CO_2 hydrogenation reactions [15–17]. One drawback of Fe is its transformation into inactive iron carbide (Fe_xC) and subsequent carbon deposition when exposed to CO_2 hydrogenation conditions [18]. Iron carbide is active for the subsequent hydrogenation of CO into hydrocarbons, since it favours C–H chain growth [19]. However, even though the FeC_x phase has been shown to be reversible, it remains a challenge to ensure the initial step of CO_2 activation on the FeO_x phase [15,20].

* Corresponding author.
E-mail address: elena.baranova@uottawa.ca (E.A. Baranova).

https://doi.org/10.1016/j.elecom.2020.106824
Received 24 July 2020; Received in revised form 21 August 2020; Accepted 22 August 2020
Available online 26 August 2020

In our previous study [21], we controlled the formation of Fe carbide in operando conditions through the Electrochemical Promotion of Catalysis (EPOC), also known as Non-Faradaic Electrochemical Modification of Catalytic Activity (NEMCA), by electrochemically supplying/removing oxygen ion species during the reaction over FeO_x/YSZ catalyst [22,23]. In a typical EPOC experiment, the catalyst acts as the working electrode in contact with a solid electrolyte. Through the application of a potential difference between the catalyst working electrode and a catalytically inert counter electrode, ionic species in the solid electrolyte can migrate through the solid electrolyte–gas–catalyst phase boundary to and away from the catalyst surface. This effect has been observed for over 100 reactions, including a handful of CO_2 hydrogenation reactions where Rh, Pd, Ru, RuCo and Ru/Co_3O_4 catalysts deposited on YSZ, Na-β″-Al_2O_3, K-β″-Al_2O_3 and BZY were evaluated [24–30].

Herein, we modified FeO_x nanowires with Ru clusters to form a Ru/FeO_x bi-phase catalyst for the RWGS reaction. We carried out STEM characterizations for the fabricated and used Ru/FeO_x and catalytic testing under open-circuit and EPOC conditions at 300–400 °C. Anodic and cathodic polarization were conducted under stoichiometric (CO_2:H_2 = 1:1) and reducing (CO_2:H_2 = 1:7) conditions to evaluate the change in catalytic behaviour. Furthermore, we studied the effect of persistent or permanent EPOC [31] over Ru/FeO_x catalysts at 400 °C under reducing conditions.

2. Experimental

The Ru/FeO_x catalyst used in this study was synthesized through a two-step polyol method. The first step consisted of fabricating FeO_x nanowires by mixing iron (III) nitrate ($Fe(NO_3)_3$) (nanohydrate, Fischer Scientific) with ethylene glycol (EG) and tetramethylammonium hydroxide (TMAOH) as described earlier [21]. EG acts as the reaction medium and reducing agent, and TMAOH is used to increase the pH of the solution, which serves as a means of controlling the size of the produced nanoparticles. The second step consisted of preparing a solution containing ruthenium chloride ($RuCl_3$) (anhydrous, Sigma Aldrich) by mixing the precursor with TMAOH, for a final pH of 12, then adding ethylene glycol to reach the desired volume. The obtained Ru precursor salt solution was then mixed with the FeO_x nanowire solution and then TMAOH was added to reach a pH of 12. After that, the solution was stirred at room temperature for 30 min, refluxed for 3 h at 160 °C and cooled down to room temperature. The final mixture was dark brown in color with a pH of ~ 7.5. The nominal atomic composition of the catalyst was 20 to 80 at. % of Ru to FeO_x.

The Ru/FeO_x catalyst was analyzed through scanning transmission electron microscopy (STEM) before and after reaction. Energy-Dispersive X-ray spectroscopy (EDX) was used to study the used sample after reaction. A FEI Titan^3 80–300 TEM operated at 300 keV, equipped with a CEOS aberration corrector (for the probe-forming lens) and an EDX spectrometer (EDAX Analyzer, DPP-II) were used. The samples were prepared following a procedure reported previously [21].

The YSZ (8 mol% Y_2O_3-stabilized ZrO_2 (Tosoh)) solid electrolyte disc (diameter = 19 mm and thickness = 1 mm) was fabricated as described elsewhere [32]. One side of the disc was painted with a counter and reference electrode made of a gold (Au) paste (C2090428D4, Gwent Group, CAS: 98–55-5), resulting in surface areas (SA) of 1 and 0.2 cm^2, respectively. The Ru/FeO_x catalyst working electrode (SA = 1 cm^2) was deposited on YSZ directly opposing the counter electrode using 10 μL of a colloidal solution at a time, and heating at 130 °C between depositions. The final catalyst loading was 0.5 mg/cm^2. A gold mesh was mechanically pressed onto the catalyst to act as a current collector.

The total flow rate of 100 mL min^{-1} consisted of CO_2 (Linde, 99.99%), H_2 (Linde, 100%) and He (Linde, 100%) at 1.5 kPa, 1.5–10.5 kPa and 88–97 kPa, respectively. The gases were fed to the reactor through three independent mass flow controllers (MFC, MKS Instruments). The same pre-treatment procedure with O_2 (20 kPa) for 2 h, followed by He purging for 15 min and then H_2 (30% in He) for 2 h at 300 °C, was performed in the electrochemical cell as described previously [21]. CO_2:H_2 ratios of 1:1 and 1:7 were examined to compare stoichiometric and reducing conditions, respectively. The product gases were analyzed using a quadrupole mass spectrometer (QMS, Ametek Proline DM 100). Potential differences and currents were applied using three gold wires connecting the working, counter and reference electrodes to the potentiostat–galvanostat (Arbin Instruments, MSTAT).

The EPOC effect was evaluated using the enhancement ratio (ρ) (eq. (1)), apparent Faradaic efficiency (Λ) (eq. (2)) and persistent EPOC ratio (γ) (eq. (3)).

$$\rho = \frac{r}{r_o} \tag{1}$$

$$\Lambda = \frac{\Delta r}{\frac{I}{zF}} \tag{2}$$

$$\gamma = \frac{r_{P-EPOC}}{r_o} \tag{3}$$

where r_o and r represent the open and closed-circuit catalytic rates, respectively, and $r_{P\text{-}EPOC}$ is the maximum open-circuit rate after potential/current interruption. The denominator in eq. (2) represents the rate at which $O^{\delta-}$ are supplied/removed through the three-phase boundary to and from Ru/FeO_x, where z is the number of electrons transferred ($2e^-$ for CO), F is Faraday's constant and I is the applied current.

3. Results and discussion

3.1. Characterization

STEM images of fresh (just prepared) and used (after reaction) Ru/FeO_x catalyst are shown in Fig. 1(a) and (b), respectively. In agreement with our earlier results [21], the FeO_x nanowires have a diameter of 5 nm and range in length from 5 to 50 nm, while the average size of the Ru clusters is ~ 1 nm [29]. The morphology shows Ru clusters supported on FeO_x, which will be denoted as Ru/FeO_x. Fig. 1(b) shows Ru/FeO_x after reaction, where various FeO_x planes are exposed: Fe_3O_4 (1 1 1), FeO (1 1 1) and FeO (2 2 0), corresponding with d-spacings of 4.8 Å, 2.5 Å and 1.6 Å, respectively [33,34]. The size of FeO_x does not significantly increase, even though the particles have agglomerated. Ru is indistinguishable, but can be associated with an amorphous structure represented by the bright area in Fig. 1(b) (circled by a red dashed line). The presence of Ru is confirmed through EDX analysis (see Fig. 1(c-f)), while the elemental Cu and Mo originate from the sample holder.

3.2. Open-circuit catalytic activity

To establish the effect of Ru on FeO_x, we compared the catalytic activity of FeO_x and Ru/FeO_x for CO_2:H_2 ratios of 1:1 and 1:7 (Fig. 2(a) and (b), respectively). In Fig. 2(a), the catalytic activity of FeO_x reached a maximum CO rate at 300 °C, followed by a lower CO rate at 335 °C which then increased with temperature. The catalytic activity associated with Ru/FeO_x increased with temperature, overtaking the CO rate of FeO_x at ~ 330 °C. Increasing the reducing conditions to CO_2:7H_2 (Fig. 2(b)) results in a similar pattern for FeO_x with a decrease in overall catalytic activity, where the CO rate reached a maximum at 300 °C, decreased at 350 °C and then increased with temperature. Ru/FeO_x outperformed FeO_x at ~ 325 °C and continued to do so up to 400 °C. Our previous works show that free-standing Ru nanoparticles produce CH_4 when used as a nanofilm deposited on YSZ and barium-zirconate yttria (BZY) solid electrolytes [21,30]. Thus, when combined with FeO_x the methanation reaction is inhibited, causing the catalytic activity to be > 99% selective for CO.

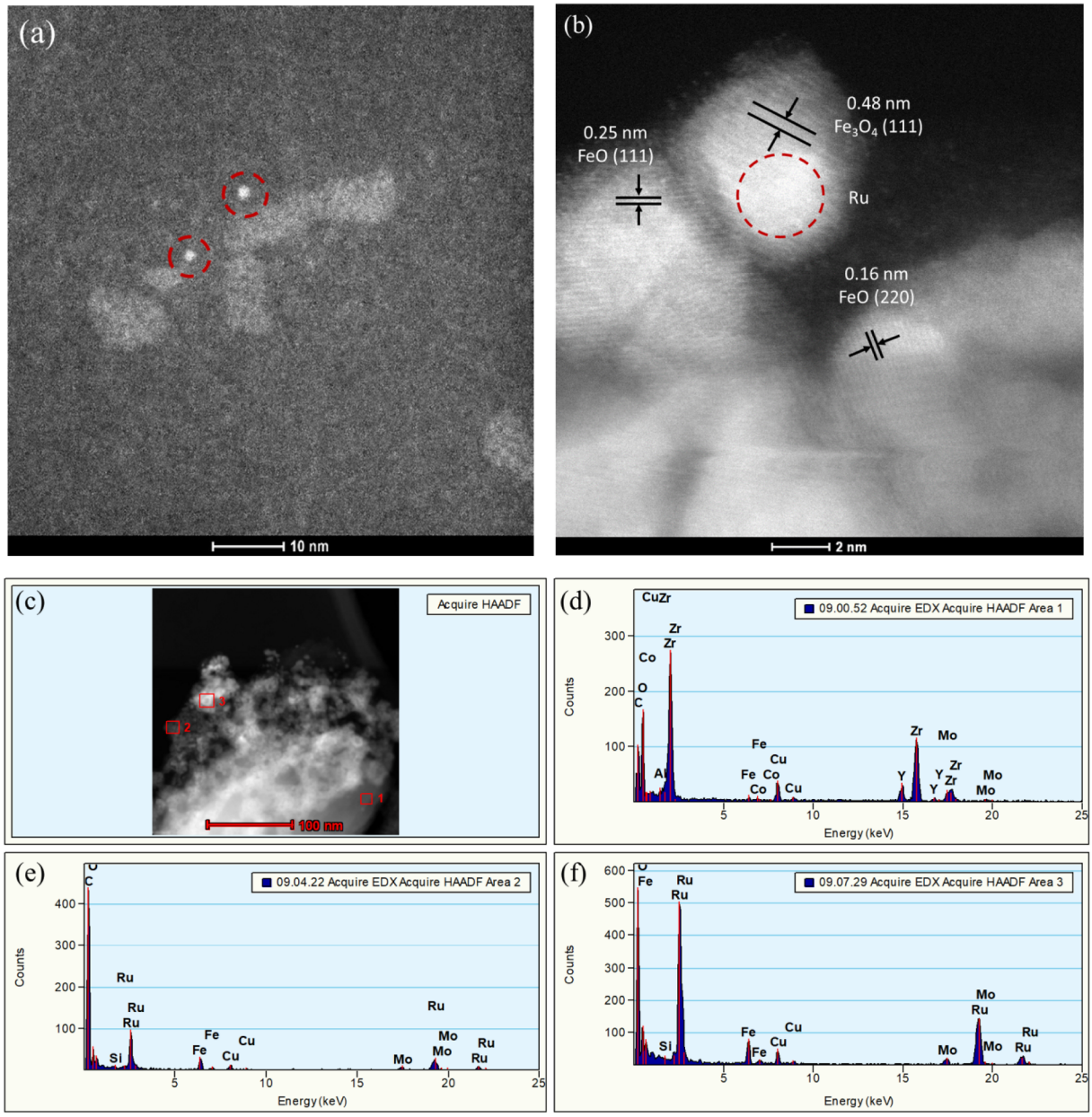

Fig. 1. STEM image of (a) a fresh colloidal solution of Ru clusters on Fe oxide nanowires and (b) spent Ru/FeO_x on YSZ, where Ru is represented by the bright spots circled by a dashed red line. EDX mapping (c) and the corresponding compositions (d)-(f) for the red squares marked in (c).

The initial high reaction rate of monometallic FeO_x is linked to the existence of an Fe_3O_4 active phase at 300 °C, which is reduced to a mixture of Fe_3O_4–FeO as the temperature is increased. In terms of Ru/FeO_x, the CO rate follows the same trend for both 1:1 and 1:7, which is to increase as a function of temperature. The increased CO rate associated with Ru/FeO_x is due to the synergetic effect between Ru and FeO_x, in which Ru has the ability to dissociate H_2 into atomic H, providing the opportunity for a spillover onto the FeO_x nanowires, thus generating oxygen vacancies. FeO_x acts as a catalyst for the adsorption of CO_2 and its subsequent cleavage into CO and O. The dissociated O is used to fill the oxygen vacancies to repeat the process all over again [35]. Thus, for monometallic FeO_x, all sites compete for the activation of CO_2 and H_2, while the addition of Ru provides sites for H_2 adsorption.

3.3. Electrochemical promotion of Ru/FeO_x

Given that the RWGS is an endothermic reaction, the electrochemical promotion experiments were undertaken at 350 and 400 °C. Fig. 3(a) shows the transient response for an applied potential of 1.5 V at 350 °C with CO_2:H_2 = 1:1. Upon anodic polarization of the Ru/FeO_x catalyst, oxygen ions migrate from YSZ to the Ru/FeO_x catalyst electrode, resulting in a CO rate increase of up to 1.6 times with an apparent Faradaic efficiency $\Lambda = 3$. When the potential was interrupted, the CO rate returned to the initial O.C. rate value.

Cathodic polarization resulted in the migration of O^{2-} from Ru/FeO_x through YSZ to the Au counter electrode. Fig. 3(b) shows the rate response upon negative −1.5 V polarization, which led to a CO rate increase of 2.4 with $\Lambda = 0.5$. Under polarization for 2 h, the reaction rate

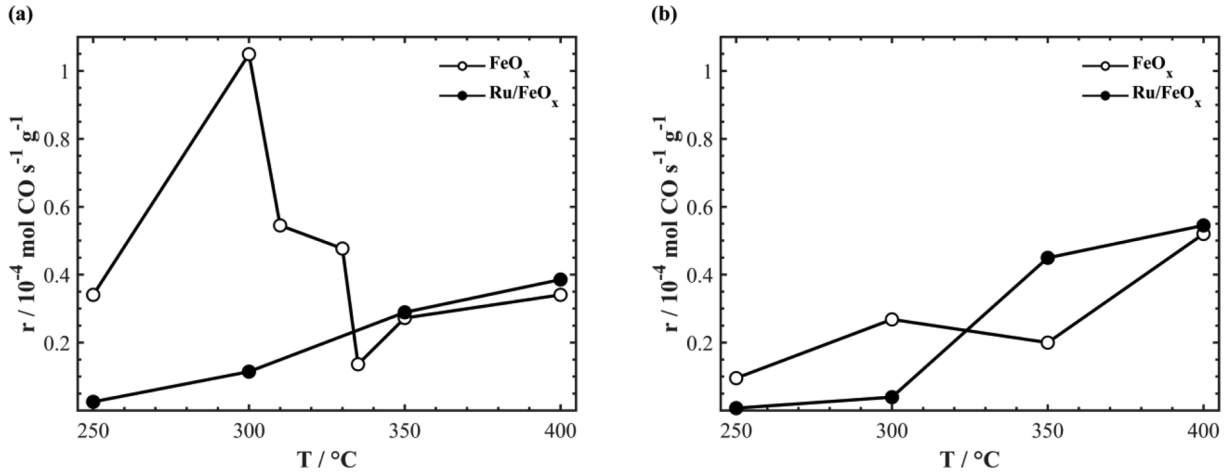

Fig. 2. Summary of the open-circuit catalytic rate on FeO_x/YSZ [21] and Ru/FeO_x/YSZ. The CO_2:H_2 ratios were (a) 1:1 and (b) 1:7.

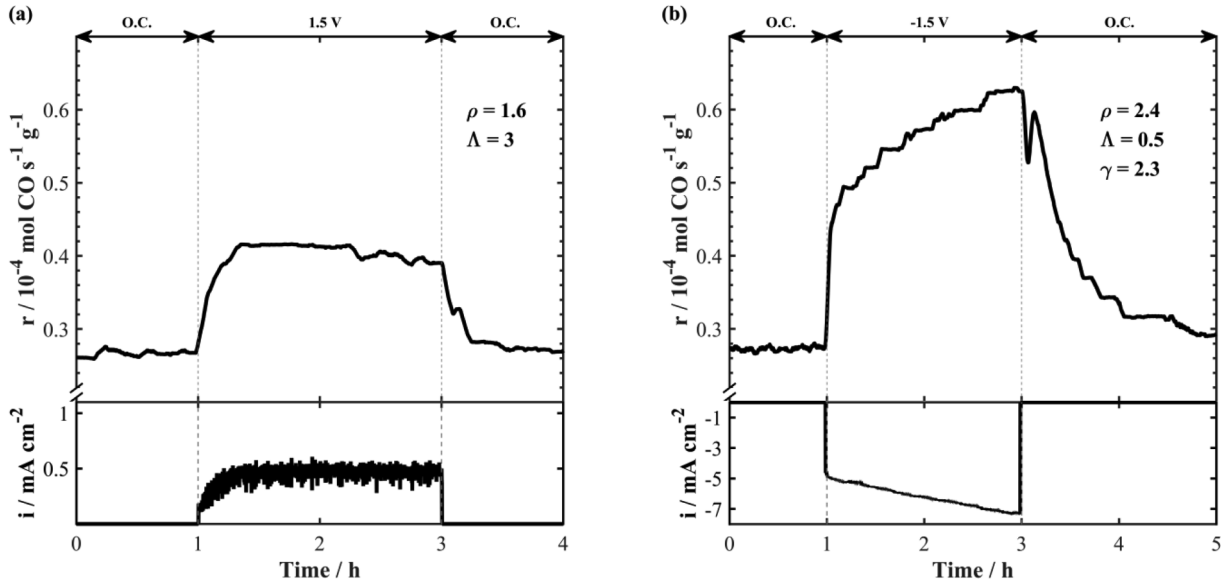

Fig. 3. Transient reaction rate response of Ru/FeO_x upon anodic (a) 1.5 V and cathodic (b) −1.5 V applied potential with CO_2:H_2 = 1:1 at 350 °C.

gradually increased due to the reduction of FeO_x, thus influencing the adsorption of CO_2 and subsequent dissociation into CO and O. After current interruption the rate remained in a promoted state (γ = 2.3) and another 2 h were required for it to return to its less active FeO_x initial state. Thus, based on the EPOC rules established by Brosda et al. [36], both positive and negative polarization resulted in an increase in the CO rate corresponding to inverted volcano behaviour, associated with weak adsorption of the electron donor (H_2) and acceptor (CO_2) on the catalyst surface [26].

The catalytic activity of Ru/FeO_x with stoichiometric (CO_2:H_2 = 1:1) and reducing (CO_2:H_2 = 1:7) gas compositions was evaluated under galvanostatic conditions at 400 °C. Fig. 4(a) displays the catalytic response under stoichiometric conditions when 1 mA current is applied. The CO rate initially increased due to the oxidation of inactive Fe_xC [21] – this stage lasts for ~ 9 min before it stabilizes in a promoted state with ρ = 1.2 and Λ = 1.04. Once the current is interrupted, oxygen stored in the form of FeO_x is made available for the reaction, resulting in an increased reaction rate and a persistent EPOC value of γ = 1.6 for 1 h before it returns to the O.C. value. For an applied current of −1mA (Fig. 4(b)), after 1 h the CO rate increased with ρ = 1.2 and Λ = 0.6. When the current is interrupted at 2 h, the p-EPOC is γ = 1.4 and requires 30 min to return to the O.C. value.

Fig. 4(c) and (d) display the effect of reducing conditions (ratio of CO_2:$7H_2$) with applied currents of 1 and –1 mA, respectively. Fig. 4(c) shows that positive current application leads to a constant increase in the CO rate with ρ = 1.4 and Λ = 2.2. Once current is interrupted at 3 h, there is p-EPOC (γ = 2.3) for 1 h before it returns to the O.C. value. This is similar behaviour to FeO_x when used on its own at 400 °C for CO_2:H_2 = 1:1 [21]. Fig. 4(d) displays the transient response under negative current –1 mA, with a steady-state rate increase of 1.2 with a Λ value of 3.4. When the current is interrupted there is a slight p-EPOC (γ = 1.3), which lasts less than 5 min. The high potential response is due to the decrease in oxygen ion conductivity of YSZ after extended catalytic testing. Because oxygen ions act as sacrificial promoters during the EPOC experiments they are continuously consumed and not replaced due to the absence of oxygen in the reaction feed. This therefore leads to YSZ reduction and a decrease in its conductivity. Regeneration of the YSZ by exposing it to an oxygen atmosphere could be envisaged in practical applications.

To elucidate the persistent EPOC effect occurring after current interruption at 400 °C, Ru/FeO_x catalysts were polarized for 5, 15 and 30 min (see Fig. 5). Between each polarization, the open-circuit conditions were maintained for 2 h to ensure that the reaction rate is at a steady state. The slight initial increase in the CO rate occurring in all

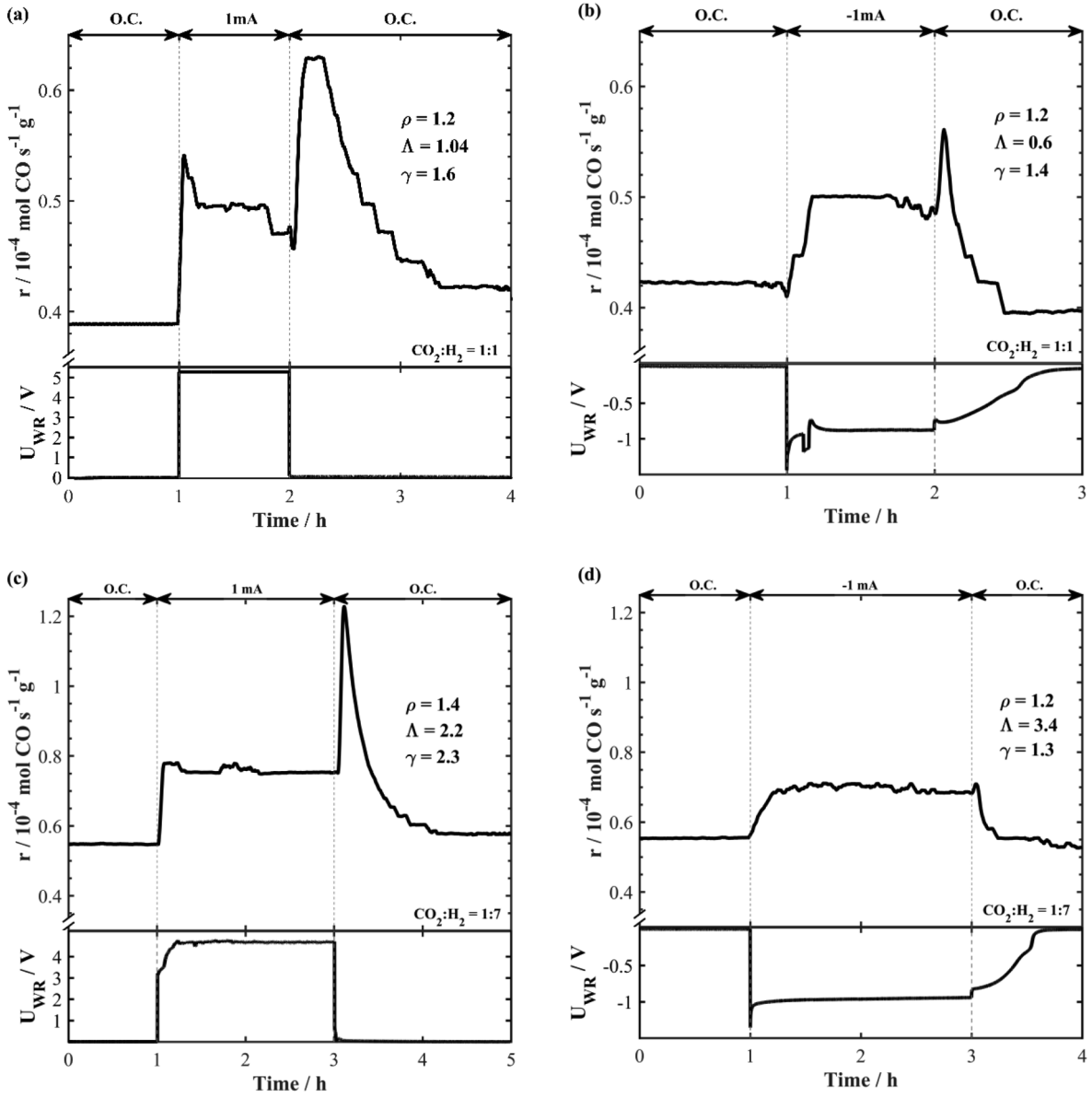

Fig. 4. Transient rate responses of Ru/FeO_x under galvanostatic conditions at 400 °C: left-hand side (a,c) + 1 mA and right-hand side (b,d) –1 mA. The gas composition is indicated in each panel.

cases can be attributed to the oxidation of the Fe_xC phase, which forms in small amounts compared to monometallic FeO_x [21] due to the presence of Ru clusters which inhibit the formation of iron carbide. The longer the polarization time, the greater the storage of oxygen in FeO_x, resulting in a longer persistent EPOC once the current is interrupted. The corresponding persistent enhancement ratios are γ_{5min} = 1.3, γ_{15min} = 1.35, and γ_{30min} = 1.5. Similar conclusions were drawn for monometallic FeO_x, indicating that FeO_x is an active component.

3.4. Effect of adding Ru

The addition of Ru to FeO_x results in a dual functioning catalyst, where Ru acts as a site for H_2 adsorption and FeO_x for CO_2 adsorption and dissociation [13,35]. The dissociation of H_2 on Ru allows for controlled H spillover onto FeO_x. A metal–support interaction effect is established between Ru clusters and FeO_x which improves the CO rate at increased temperature and results in new electrochemical behaviour. A direct comparison of Ru/FeO_x and FeO_x is shown in Figs. S1 and S2. Although Ru influences the reaction rate, the FeO_x prevails, ensuring that the selectivity for CO is > 99%.

Compared with monometallic FeO_x, the absence of an initial CO rate increase once the anodic potential or current is applied indicates that a negligible amount of the Fe_xC phase is formed in Ru/FeO_x [21]. This is further confirmed in the STEM image in Fig. 1(b), which shows that the proximity of Ru to the FeO_x facets influences its oxidation state: Fe_3O_4 (111) is present near Ru, while FeO (111) and FeO (220) facets are exposed when Ru is absent. Furthermore, no carbon was detected on the STEM images, unlike the monometallic FeO_x which forms a FeO_x-C core–shell structure [21]. This suggests that Ru inhibits the formation of iron carbide (Fe_xC) by providing active sites for H_2 adsorption and dissociation, with H remaining on Ru, halting the reduction of FeO_x into Fe_xC. Figure S3 compares the ρ_{max} values of Ru/FeO_x and FeO_x, which are associated with the formation of Fe carbide.

Ru/FeO_x shows new p-EPOC behaviour compared to FeO_x under negative polarization, which indicates that the adsorption strength of H on Ru is weakened [29,37]. The weakening of the H bond and increase in CO_2 activation on FeO_x allow H to spillover from Ru to reduce FeO_x sites without both reactants competing for the same sites. FeO_x is

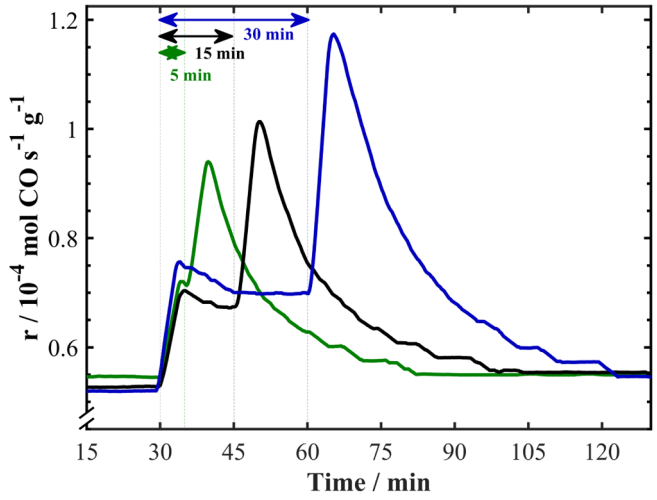

Fig. 5. Transient rate response to application of 1 mA for 5, 15 and 30 min at CO_2:H_2 = 1:7 and 400 °C.

reduced to an active state during the polarization that persists after current interruption before returning to its initial less active FeO_x state.

4. Conclusions

Our findings show that addition of Ru clusters to FeO_x decreases the formation of inactive FeC_x, as confirmed in open-circuit and EPOC experiments. Ru is shown to improve the redox reaction taking place on FeO_x by adsorbing H_2 and supplying H to FeO_x, in the temperature range 250–400 °C. A synergistic effect occurs between Ru and FeO_x, which enables FeO_x to remain in an active state for the RWGS reaction (> 99% selective to CO) and increase by 2.4 times during polarization. Overall, the addition of Ru nanoparticles in a two-step synthesis enhances FeO_x performance in redox reactions that can be applied to industrial scale applications where catalytic stability and susceptibility to carbide formation are crucial.

CRediT authorship contribution statement

Christopher Panaritis: Conceptualization, Methodology, Investigation, Data curation, Writing - original draft, Writing - review & editing, Visualization. **Johnny Zgheib:** Validation, Investigation. **Martin Couillard:** Resources. **Elena A. Baranova:** Supervision, Data curation, Writing - review & editing, Project administration, Funding acquisition.

Declaration of Competing Interest

The authors declare that they have no known competing financial interests or personal relationships that could have appeared to influence the work reported in this paper.

Acknowledgments

This work was supported by the Natural Sciences and Engineering Research Council of Canada (NSERC) Discovery Grant (RGPIN05494).

Appendix A. Supplementary data

Supplementary data to this article can be found online at https://doi.org/10.1016/j.elecom.2020.106824.

References

[1] W. Steffen, et al., Proc. Natl. Acad. Sci. USA 115 (2018) 8252–8259.
[2] M.D. Porosoff, B. Yan, J.G. Chen, Energy Environ. Sci. 9 (2016) 62–73.
[3] S. Saeidi, S. Najari, F. Fazlollahi, M.K. Nikoo, F. Sefidkon, J.J. Klemeš, L.L. Baxter, Renew. Sustain. Energy Rev. 80 (2017) 1292–1311.
[4] C. Hepburn, E. Adlen, J. Beddington, E.A. Carter, S. Fuss, N. MacDowell, J.C. Minx, P. Smith, C.K. Williams, Nature 575 (2019) 87–97.
[5] D.C. Upham, A.R. Derk, S. Sharma, H. Metiu, E.W. McFarland, Catal, Sci. Technol. 5 (2015) 1783–1791.
[6] Y. Yan, Q. Wang, C. Jiang, Y. Yao, D. Lu, J. Zheng, Y. Dai, H. Wang, Y. Yang, J. Catal. 367 (2018) 194–205.
[7] K. Zhao, L. Wang, M. Calizzi, E. Moioli, A. Züttel, J. Phys. Chem. C 122 (2018) 20888–20893.
[8] J.H. Kwak, L. Kovarik, J. Szanyi, ACS Catal. 3 (2013) 2449–2455.
[9] C. Panaritis, M. Edake, M. Couillard, R. Einakchi, E.A. Baranova, J. CO2 Util. 26 (2018) 350–358.
[10] P. Vernoux, L. Lizarraga, M.N. Tsampas, F.M. Sapountzi, A. De Lucas-Consuegra, J.L. Valverde, S. Souentie, C.G. Vayenas, D. Tsiplakides, S. Balomenou, E.A. Baranova, Chem. Rev. 113 (2013) 8192–8260.
[11] K. Chang, H. Zhang, M.J. Cheng, Q. Lu, ACS Catal. 10 (2020) 613–631.
[12] M. Boaro, S. Colussi, A. Trovarelli, Front. Chem. 7 (2019) 28.
[13] S. Kattel, P. Liu, J.G. Chen, J. Am. Chem. Soc. 139 (2017) 9739–9754.
[14] M. Wenzel, N.V.R. Aditya Dharanipragada, V.V. Galvita, H. Poelman, G.B. Marin, L. Rihko-Struckmann, K. Sundmacher, J. CO2 Util. 17 (2017) 60–68.
[15] D.H. Kim, S.W. Han, H.S. Yoon, Y.D. Kim, J. Ind. Eng. Chem. 23 (2014) 67–71.
[16] J.A. Rodriguez, P. Liu, D.J. Stacchiola, S.D. Senanayake, M.G. White, J.G. Chen, ACS Catal. 5 (2015) 6696–6706.
[17] M.V. Landau, N. Meiri, N. Utsis, R. Vidruk Nehemya, M. Herskowitz, Ind. Eng. Chem. Res. 56 (2017) 13334–13355.
[18] S.C. Lee, J.S. Kim, W.C. Shin, M.J. Choi, S.J. Choung, J. Mol. Catal. A Chem. 301 (2009) 98–105.
[19] R.W. Dorner, D.R. Hardy, F.W. Williams, H.D. Willauer, Energy Environ. Sci. 3 (2010) 884–890.
[20] J.A. Loiland, M.J. Wulfers, N.S. Marinkovic, R.F. Lobo, Catal. Sci. Technol. 6 (2016) 5267–5279.
[21] C. Panaritis, J. Zgheib, S.A.H. Ebrahim, M. Couillard, E.A. Baranova, Appl. Catal. B Environ. 269 (2020) 118826.
[22] C.G. Vayenas, S. Bebelis, C. Pliangos, S. Brosda, D. Tsiplakides, Electrochemical Activation of Catalysis: Promotion, Electrochemical Promotion, Metal-Support Interaction, Kluwer Academic/Plenum, New York, 2001.
[23] G.G. Vayenas, S. Bebelis, S. Ladas, Nature 343 (1990) 625–627.
[24] S. Bebelis, H. Karasali, C.G. Vayenas, J. Appl. Electrochem. 38 (2008) 1127–1133.
[25] S. Bebelis, H. Karasali, C.G. Vayenas, Solid State Ionics 179 (2008) 1391–1395.
[26] D. Theleritis, S. Souentie, A. Katsaounis, C.G. Vayenas, ACS Catal. 2 (2012) 770–780.
[27] I. Kalaitzidou, M. Makri, D. Theleritis, A. Katsaounis, C.G. Vayenas, Surf. Sci. 646 (2016) 194–203.
[28] A. Kotsiras, I. Kalaitzidou, D. Grigoriou, A. Symillidis, M. Makri, A. Katsaounis, C.G. Vayenas, Appl. Catal. B Environ. 232 (2018) 60–68.
[29] C. Panaritis, C. Michel, M. Couillard, E.A. Baranova, S.N. Steinmann, Electrochim. Acta 350 (2020) 136405.
[30] D. Zagoraios, C. Panaritis, A. Krassakopoulou, E.A. Baranova, A. Katsaounis, C.G. Vayenas, Appl. Catal. B Environ. 276 (2020) 119148.
[31] C. Falgairette, A. Jaccoud, G. Fóti, C. Comninellis, J. Appl. Electrochem. 38 (2008) 1075–1082.
[32] I.R. Gibson, G.P. Dransfield, J.T.S. Irvine, J. Mater. Sci. 33 (1998) 4297–4305.
[33] B. Leszczynski, G.C. Hadjipanayis, A.A. El-Gendy, K. Załęski, Z. Śniadecki, A. Musial, M. Jarek, S. Jurga, A. Skumiel, J. Magn. Magn. Mater. 416 (2016) 269–274.
[34] A. Lak, J. Dieckhoff, F. Ludwig, J.M. Scholtyssek, O. Goldmann, H. Lünsdorf, D. Eberbeck, A. Kornowski, M. Kraken, F.J. Litterst, K. Fiege, P. Mischnick, M. Schilling, Nanoscale. 5 (2013) 11447–11455.
[35] D. Zhang, J. Luo, J. Wang, X. Xiao, Y. Liu, W. Qi, D.S. Su, W. Chu, Chinese, J. Catal. 39 (2018) 157–166.
[36] S. Brosda, C.G. Vayenas, J. Wei, Appl. Catal. B Environ. 68 (2006) 109–124.
[37] D. Theleritis, S. Souentie, A. Siokou, A. Katsaounis, C.G. Vayenas, ACS Catal. 2 (2012) 770–780.